

Published in final edited form as:

J Inorg Biochem. 2011 April ; 105(4): 538–547. doi:10.1016/j.jinorgbio.2010.12.006.

Deconvolution of Raman spectroscopic signals for electrostatic, H-bonding, and inner-sphere interactions between ions and dimethyl phosphate in solution

Eric L Christian^{*,a,b}, Vernon E. Anderson^{b,c}, and Michael E Harris^{a,b}

^aCenter for RNA Molecular Biology, Case Western Reserve University School of Medicine, Cleveland Ohio, 44106

^bDepartment of Biochemistry, Case Western Reserve University School of Medicine, Cleveland Ohio, 44106.

Abstract

Quantitative analysis of metal ion-phosphodiester interactions is a significant experimental challenge due to the complexities introduced by inner-sphere, outer-sphere (H-bonding with coordinated water), and electrostatic interactions that are difficult to isolate in solution studies. Here, we provide evidence that inner-sphere, H-bonding and electrostatic interactions between ions and dimethyl phosphate can be deconvoluted through peak fitting in the region of the Raman spectrum for the symmetric stretch of non-bridging phosphate oxygens ($\nu_s\text{PO}_2^-$). An approximation of the change in vibrational spectra due to different interaction modes is achieved using ions capable of all or a subset of the three forms of metal ion interaction. Contribution of electrostatic interactions to ion-induced changes to the Raman $\nu_s\text{PO}_2^-$ signal could be modeled by monitoring attenuation of $\nu_s\text{PO}_2^-$ in the presence of tetramethylammonium, while contribution of H-bonding and inner-sphere coordination could be approximated from the intensities of altered $\nu_s\text{PO}_2^-$ vibrational modes created by an interaction with ammonia, monovalent or divalent ions. A model is proposed in which discrete spectroscopic signals for inner-sphere, H-bonding, and electrostatic interactions are sufficient to account for the total observed change in $\nu_s\text{PO}_2^-$ signal due to interaction with a specific ion capable of all three modes of interaction. Importantly, the quantitative results are consistent with relative levels of coordination predicted from absolute electronegativity and absolute hardness of alkali and alkaline earth metals.

Keywords

Dimethyl phosphate; Metal Ion; Ion binding; Raman Spectroscopy

1. Introduction

Metal ion interactions with phosphate groups are an essential and ubiquitous component of biological systems and are necessary for the proper folding of structural RNAs and often

© 2010 Elsevier Inc. All rights reserved.

*Correspondence; eric.christian@case.edu, phone 216-368-1877..

^cCurrent address: National Institute of General Medical Sciences, Building 45 - Natcher Building, 2AS43J, 45 Center Dr., Bethesda, MD 20892

Publisher's Disclaimer: This is a PDF file of an unedited manuscript that has been accepted for publication. As a service to our customers we are providing this early version of the manuscript. The manuscript will undergo copyediting, typesetting, and review of the resulting proof before it is published in its final citable form. Please note that during the production process errors may be discovered which could affect the content, and all legal disclaimers that apply to the journal pertain.

serve as essential cofactors for catalysis of phosphoryl transfer by both RNA and protein enzymes[1-4]. These interactions include electrostatic charge-charge interactions between a positively charged metal and the negatively charged phosphodiester backbone, outer-sphere coordination involving hydrogen bonding (H-bonding) via coordinated water molecules, and inner-sphere coordination with electronegative groups on RNA (Figure 1) [5, 6]. Experimental detection and quantification of individual modes of ion interaction, however, are difficult due to the diversity of chemical interactions and geometries and the linkage between ion binding and conformational changes during RNA folding[7, 8].

Raman spectroscopy has been proposed recently for the quantitative and semi-quantitative analysis of metal phosphate interactions[9, 10]. Individual peaks within the Raman spectrum are determined by the normal modes of bond vibrations, many of which are dominated by individual groups of bonded atoms[11, 12]. The intensity and wavenumber of the Raman shift is highly sensitive to changes in chemical bonding environment of the vibrating atoms. Therefore, interactions with metal ions that induce differences in bonding necessarily result in changes in the Raman spectrum. Application of this method for detecting metal ion interactions with nucleic acids and other biological phosphodiester, however, has been limited primarily by the lack of quantitative frameworks for interpreting spectral changes in terms of specific ion interactions.

Studies of metal-dependent changes in the Raman spectra of phosphodiester from dimethyl phosphate (DMP) to larger nucleic acids consistently note a significant change in the vibration frequency of the symmetric stretch of the non-bridging phosphate oxygens ($\nu_s\text{PO}_2^-$), which shifts to higher frequency in the Raman spectrum in the presence of metal cations[13]. The degree of metal-induced change in $\nu_s\text{PO}_2^-$ vibrational frequency is insensitive to metal ion concentration and is consistent with a discrete rather than a progressive displacement of $\nu_s\text{PO}_2^-$ to higher wavenumbers upon metal ion binding[9]. The displacement $\nu_s\text{PO}_2^-$ to higher wavenumbers in the presence of metal ions appears as an inflection in difference spectra, and is observed for all metal ions typically associated with biological systems[9, 13-17].

Recent computational studies of DMP binding to Mg^{2+} and Ca^{2+} predict a shift of $\nu_s\text{PO}_2^-$ to higher wavenumbers resulting from metal coordination[18]. Consistent with this prediction, the intensity of the $\nu_s\text{PO}_2^-$ inflection induced by Mg^{2+} was shown in Raman spectra of RNA crystals to correlate with the loss of vibrational modes characteristic of fully hydrated magnesium ion $[\text{Mg}(\text{H}_2\text{O})_6]$ and formation of magnesium penta or tetrahydrate, implying a change in the interactions of phosphate with aqueous solvent by the displacement of magnesium bound water in favor of binding to non-bridging phosphate oxygens[10]. In solution, the displacement of $\nu_s\text{PO}_2^-$ to higher wavenumbers has recently shown to be due to purely inner-sphere coordination, while the metal-induced attenuation of $\nu_s\text{PO}_2^-$ signal intensity is due contribution from all three forms of metal ion interaction[9]. The same partition in the contributions of electrostatic, H-bonding, and inner-sphere coordination to the observed changes in $\nu_s\text{PO}_2^-$ signal is observed for a wide range of phosphodiester from simple model compounds (*e.g.* DMP) to structurally complex RNAs (*e.g.* yeast tRNA^{PHE}), and thus appears to reflect a fundamental spectroscopic property of phosphodiester[9].

Isolation of a spectroscopic signal for inner-sphere coordination provides a number of useful tools for the study of metal-phosphodiester interactions. Analysis of the intensity of the $\nu_s\text{PO}_2^-$ signal displaced to higher wavenumbers as a function of metal ion concentration was shown to accurately measure divalent metal ion (Mg^{2+}) binding stoichiometry to ATP and ADP[9]. In addition, different metal ions alter the displacement of the perturbed $\nu_s\text{PO}_2^-$ vibrational mode ($\nu_s\text{PO}_2\text{M}$) to different extents, and are strongly influenced by absolute electronegativity and absolute hardness. For many metal ions, the change in $\nu_s\text{PO}_2^-$

frequency upon binding ($\Delta\nu_M$) is sufficient to confirm metal ion identity or to distinguish between metal ion interactions in a mixed metal solution[9]. However, our understanding of the extent to which electrostatic and outer-sphere metal-phosphodiester interactions can be distinguished by Raman spectroscopy has not been systematically explored. While experimental and computational studies suggest that electrostatic and H-bonding interactions can contribute significantly to the observed ion-induced changes of $\nu_s\text{PO}_2^-$ frequency[16, 18], the relative contribution of these individual forms of ion interaction have not been determined. Characterization of signals for electrostatic and outer-sphere metal-phosphodiester interactions thus remains an important goal in the development of a complete framework for the quantitative interpretation of Raman spectra as a direct experimental means of characterizing the full distribution of ion binding interactions to phosphodiesters.

Experimental evidence for a distinct $\nu_s\text{PO}_2^-$ vibrational mode associated with outer-sphere H-bonding comes from quantitative analysis of Ni^{2+} -induced changes to the Raman spectrum of diethyl phosphate (DEP)[16]. In addition to a metal-induced shift of $\nu_s\text{PO}_2^-$ to higher wavenumbers ($\sim 8\text{ cm}^{-1}$) that is associated with inner-sphere coordination, Ni^{2+} binding to DEP also produces a smaller, but significant ($\sim 3\text{ cm}^{-1}$) shift of $\nu_s\text{PO}_2^-$ to lower wavenumbers in the Raman spectrum. The metal-induced shift of $\nu_s\text{PO}_2^-$ to lower wavenumbers is predicted to reflect outer-sphere coordination based on the likelihood that increased acidity of the metal coordinated water will strengthen the hydrogen bond to the phosphate group and decrease $\nu_s\text{PO}_2^-$ vibration relative to that to the aqueous solvent in the absence of metal ion. Recent computational studies of DMP with Mg^{2+} and Ca^{2+} are consistent with this observation[16, 18]. Qualitative comparison of Ni^{2+} binding to DEP to that observed in alkali, alkaline earth, and other transition metal ions indicates that the metal-induced shift of $\nu_s\text{PO}_2^-$ to lower wavenumbers is likely to be a useful spectroscopic feature for quantifying outer-sphere coordination. Electrostatic interactions, by contrast, were predicted by quantitative experimental studies with DEP to form an additional $\nu_s\text{PO}_2^-$ vibrational mode displaced approximately 10 cm^{-1} to higher wavenumbers[16]. Prediction of a greater frequency change of $\nu_s\text{PO}_2^-$ for electrostatic versus outer-sphere coordination, however, is inconsistent with a general observation from theoretical studies that smaller changes in $\nu_s\text{PO}_2^-$ are expected with increasing distance between metal ion and DMP and indicates that further experiments are required to resolve this issue[18].

In the current work, we attempt to deconvolute the relative contribution of outer-sphere, inner-sphere, and electrostatic interactions to ion-induced changes in the Raman spectrum of DMP using ions capable of all, or a subset of these three forms of metal ion interaction. Additionally, we compare apparent levels of coordination at equal ionic strength for a range of alkali, alkaline earth and transition metal ions. We define a minimal model for spectroscopic signals that correlates with electrostatic, outer-sphere, and inner-sphere interactions, and is sufficient to account for the total ion-dependent loss of $\nu_s\text{PO}_2^-$ intensity in DMP. These studies provide an initial, simple framework for the quantitative interpretation of Raman spectra in terms of the spectroscopic signals for the three individual modes of metal-phosphodiester interactions.

2. Materials and Methods

2.1. Reagents

MnCl_2 , and sodium formate were obtained from Sigma. CaCl_2 , CoCl_2 , and ZnCl_2 , were purchased from Fisher Scientific. CdCl_2 , was obtained from Acros Organics, MgCl_2 was purchased from Ambion Inc. DMP was synthesized by hydrolysis of dimethyl chlorophosphate (Aldrich) as described previously[9].

2.2. Raman spectroscopy

Raman spectra were collected using a HoloLab Series 5000 Raman microscope (Kaiser Optical Systems). Individual samples (4 μL in the form of a hanging drop from a siliconized cover slip) were exposed to 100 mW of 647.1 nm laser excitation passed through the microscope's 20X objective lens for 300 seconds. Calibration of the Raman microscope was done using neon and tungsten lamp standards, which indicate that the variation in the positions of individual Raman bands measured on different days to be less than 1 cm^{-1} . Measurement of successive DMP samples within the same Raman experiment, however, showed variation in $\nu_s\text{PO}_2^-$ peak position of less than 0.1 cm^{-1} . All spectra were measured at ambient temperature, which varied between 20 and 25°C . Variation of the Raman signals between 20°C and 25°C for the model compounds used in these studies was indistinguishable from the observed experimental error at constant temperature. DMP (200 mM) was measured in 200 mM formate pH 6 in the absence or presence of different ions as indicated.

The effect of ion pair formation on the Raman signal was analyzed by difference spectra, in which the Raman spectrum of a phosphodiester anion with a baseline concentration of 400 mM Na^+ is subtracted from that in the added presence of an ion in question (*e.g.* Mg^{2+}), and by direct peak fitting of the observed (raw) spectral data in the absence or presence of the additional ion. DMP methyl group vibrational modes centered at 1466 cm^{-1} and 1453 cm^{-1} were used as intensity standards due to the absence of observed systematic perturbation in the presence of increasing concentrations of solution ions. All Raman difference spectra were derived from data collected within the same session of data acquisition on the Raman instrument.

Areas of peaks or peak fitting of Raman spectra were determined using GRAMS/AI software (Thermo Galactic Corp.). Specifically, Raman spectra between 980 cm^{-1} and 1140 cm^{-1} of DMP in the absence of added ion were fit to a minimum of three Voigt peaks centered at 1084 cm^{-1} , 1066 cm^{-1} , and 1045 cm^{-1} that correspond to published positions for $\nu_s\text{PO}_2^-$ and the asymmetric and symmetric C-O stretch ($\nu_a\text{CO}$ and $\nu_s\text{CO}$), respectively. Peak parameters (position, intensity, and width at half height) of $\nu_s\text{PO}_2^-$, $\nu_a\text{CO}$ and $\nu_s\text{CO}$ for DMP in the absence of added ion were then used as the initial seed values for peak fitting of DMP in the presence of tetramethylammonium $[\text{N}(\text{CH}_3)_4^+]$, in which position, intensity, and width at half height were allowed to vary independently. Peak parameters of DMP in the presence of $\text{N}(\text{CH}_3)_4^+$ were then used as the initial seed values for peak fitting of DMP in the presence of NH_4^+ or Mg^{2+} at equal ionic strength. When all peak parameters were allowed to vary, little change was observed in the position of $\nu_s\text{PO}_2^-$, $\nu_a\text{CO}$ and $\nu_s\text{CO}$ for DMP in the presence of NH_4^+ or Mg^{2+} relative to that observed for $\text{N}(\text{CH}_3)_4^+$ at equal ionic strength. Peak positions of $\nu_s\text{PO}_2^-$, $\nu_a\text{CO}$ and $\nu_s\text{CO}$ for DMP in the presence of NH_4^+ or Mg^{2+} were thus fixed to that observed in $\text{N}(\text{CH}_3)_4^+$ at equal ionic strength, with intensity and width at half height allowed to vary. All parameters were allowed to vary for additional peaks ($\nu_s\text{PO}_2^- \text{H}$, $\nu_s\text{PO}_2^- \text{M}$, see Results) required to fit spectra of DMP in the presence of NH_4^+ or Mg^{2+} . Experimental error of reported peak areas or position reflects the observed variation from at least three independent experiments.

3. Results

In this study we set out to define a framework for the analysis of metal-phosphodiester interactions by Raman spectroscopy by: 1. Determining if the spectroscopic signals for electrostatic and outer-sphere interactions predicted by computation could be observed in DMP; 2. Determining the quantitative relationship between ion-induced $\nu_s\text{PO}_2^-$ intensity loss and the gain of spectroscopic signals correlated with outer-sphere, and inner-sphere

interactions; and 3, Examining the relationship between metal ion identity and the modes attributable to different chemical interactions in DMP ion pairs.

DMP is a well-established model system for studying the behavior of metal ion interaction with phosphodiester monoanions, and has been shown to mimic the spectroscopic behavior of the 5', 3' phosphodiester backbone of nucleic acids[19, 20]. Like DEP, DMP has the advantage of allowing the direct comparison of the relative level of outer-sphere and inner-sphere interactions to the same phosphoryl group, which is difficult in more complex phosphodiesters (*e.g.* ATP or RNA) that have an asymmetric distribution of bound ions and involve large conformational changes coupled to ion binding. Additionally, high concentrations of DMP can be analyzed to produce a high signal to noise ratio facilitating the quantitative analysis of ion-induced changes in vibrational mode identity and intensity.

A summary of ion-induced changes in the Raman spectrum of DMP is shown in Figure 2. DMP has a simple Raman spectrum that is dominated by the vibrational modes of the methyl groups and the bridging and non-bridging phosphate oxygens (observed at 1450-^1 and 1464cm^{-1} , 1083 cm^{-1} , and 754 cm^{-1} , respectively)[19, 20]. The largest signal is that for the symmetric stretch of the non-bridging phosphate oxygens, $\nu_s\text{PO}_2^-$. Metal-induced changes in $\nu_s\text{PO}_2^-$ are readily apparent in the Raman spectrum and in the difference spectra used to isolate net changes in the spectroscopic signal resulting from the inclusion of solution ions (Figure 2B and 2C). Addition of metal ions (*e.g.* Mg^{2+}) to solutions containing 0.2 M DMP produces both a reduction in the intensity (observed photon counts) of $\nu_s\text{PO}_2^-$ at 1083 cm^{-1} and an increase in Raman signal at higher wavenumbers. As noted above, previous studies showed that the metal-induced attenuation of $\nu_s\text{PO}_2^-$ (the negative node of the difference spectrum) reflects contribution from all three forms of ion interaction, while the apparent shift of $\nu_s\text{PO}_2^-$ to higher numbers (the positive node of the difference spectrum) reflects purely inner-sphere coordination[9].

3.1. $\text{N}(\text{CH}_3)_4^+$, NH_4^+ , and Mg^{2+} -induced changes to $\nu_s\text{PO}_2^-$ reveal distinct spectroscopic contributions from electrostatic, H-bonding, and inner-sphere coordination

In order to gain additional information on changes in $\nu_s\text{PO}_2^-$ due to of electrostatic, H-bonding, and inner-sphere coordination, we compared the effects of ions capable of all or a subset of the three modes of metal ion interaction on the Raman spectrum of DMP. Specifically, we examined ion induced changes by tetramethylammonium [$\text{N}(\text{CH}_3)_4^+$], which is capable of only electrostatic interactions, and ammonium (NH_4^+) and magnesium (Mg^{2+}), which can interact through electrostatic and H-bonding interactions, or electrostatic, H-bonding, and inner-sphere interactions, respectively. Raman difference spectra in which the spectrum of DMP is subtracted from that in the presence of the added ion of interest were analyzed over a range of ion concentrations and compared to reveal changes in spectral features (Figure 3). Ion concentrations are shown in units of ionic strength to allow direct comparison of mono and divalent ions. The high ion concentrations used reflects the low affinity of the simple phosphodiester to ion binding. However, as noted above, ion-dependent changes in DMP spectra correlate well with those of other phosphodiesters (*e.g.* RNA) that bind ions with much greater affinity, and can yield changes in the Raman difference spectrum in the 1-100 mM range [9, 19-22]. Ions were compared with the understanding that ion-specific effects beyond differences in their modes of interaction with DMP are also likely to contribute to the observed Raman spectra. The extent to which ion-specific effects contribute to the $\nu_s\text{PO}_2^-$, however, is currently unknown. $\text{N}(\text{CH}_3)_4^+$, NH_4^+ , and Mg^{2+} were thus compared to determine the extent to which individual spectroscopic features for electrostatic, H-bonding, and coordination interactions can account for the observed ion-induced changes in $\nu_s\text{PO}_2^-$.

Figure 3A shows that concentration dependent changes due to $\text{N}(\text{CH}_3)_4^+$ on $\nu_s\text{PO}_2^-$ and adjacent vibrational modes in the DMP Raman difference spectrum are consistent with at least two distinct components: an increase in signal intensity between 1040 cm^{-1} to 1070 cm^{-1} and a progressive shift in signal from $\sim 1080\text{ cm}^{-1}$ (center dotted line) to higher wavenumbers with increasing $\text{N}(\text{CH}_3)_4^+$ concentration. The broad increase in Raman intensity between 1040 cm^{-1} to 1070 cm^{-1} includes the symmetric and asymmetric C-O stretches ($\nu_s\text{CO}$ and $\nu_a\text{CO}$) centered at 1045 cm^{-1} to 1066 cm^{-1} (Figure 1). The increasing spectroscopic signal at higher wavenumbers is in the region covered by $\nu_s\text{PO}_2^-$ that is centered at $\sim 1083\text{ cm}^{-1}$, and this intensity appears to progressively shift to higher wavenumbers in a concentration dependent manner.

Concentration dependent changes of $\nu_s\text{PO}_2^-$ and adjacent vibrational modes in the DMP Raman difference spectrum due to NH_4^+ produce an inflection at lower wavenumbers in the region covered by $\nu_s\text{PO}_2^-$ centered at 1083 cm^{-1} in addition to an increase in signal from 1020 cm^{-1} to 1070 cm^{-1} (Figure 3B). The position of the negative and positive peaks of the inflection ($\sim 1089\text{ cm}^{-1}$ and 1074 cm^{-1} , respectively), isolating the effect of NH_4Cl , do not change significantly as a function of NH_4^+ concentration. The observation of a concentration independent displacement of signal to toward lower wavenumbers is consistent with a discrete rather than a progressive change in $\nu_s\text{PO}_2^-$ vibrational frequency. The observation above is not unexpected since changes in the strength of individual bonds necessarily produce discrete changes in the observed Raman frequency. In particular, increased acidity of the metal coordinated water is likely strengthen the hydrogen bond to the phosphate group and decrease the vibrational frequency of $\nu_s\text{PO}_2^-$ relative to that involved in H-bonding to uncoordinated water. Indeed, displacement of $\nu_s\text{PO}_2^-$ to lower wavenumbers by H-bonding is both predicted by computation and has been observed in previous studies of DMP and DEP in the presence of metal ions[16, 18].

As observed previously for ions capable of direct coordination, concentration dependent changes of the Mg^{2+} Raman difference spectrum produce a displacement of signal to higher wavenumbers consistent with the formation of an altered $\nu_s\text{PO}_2^-$ vibrational mode as a result of inner-sphere coordination ($\nu_s\text{PO}_2^- \text{M}$) and the loss of signal intensity of $\nu_s\text{PO}_2^-$ (Figure 1C)[9]. Like the NH_4^+ -induced displacement of $\nu_s\text{PO}_2^-$ to lower wavenumbers associated with H-bonding, the magnitude of the Mg^{2+} -dependent displacement to higher wavenumbers due to coordination is concentration independent and consistent with a discrete rather than a progressive change in $\nu_s\text{PO}_2^-$ vibrational frequency. The difference spectrum isolating the effect of Mg^{2+} , however, does not display ion-dependent changes associated with electrostatic or H-bonding that occur simultaneously with inner-sphere interactions with DMP in solution (Compare Figure 3A, 3B and 3C). Similarly, NH_4^+ Raman difference spectra do not display all of the characteristic changes observed for electrostatic interactions (compare Figures 3A and 3B). The apparent absence of significant additive contribution to $\nu_s\text{PO}_2^-$ from electrostatics, H-bonding, and inner-sphere interactions is likely due in part to offsetting changes in height, width, and position of the individual vibrational modes of $\nu_s\text{PO}_2^-$, $\nu_s\text{CO}$, and $\nu_a\text{CO}$, which can be hidden during subtraction of overlapping peaks and make quantitative interpretation of Raman difference spectra difficult.

3.2. Quantitative contribution from electrostatic, H-bonding, and inner-sphere coordination can be determined by peak fitting of the observed DMP Raman spectrum

To better characterize the effect of electrostatic interactions on the Raman spectra in DMP, and $\nu_s\text{PO}_2^-$ in particular, we examined changes in peak position, height, and width at half-height (WHH) of $\nu_s\text{PO}_2^-$ and overlapping $\nu_s\text{CO}$ and $\nu_a\text{CO}$ vibrational modes in raw spectral data taken in the absence and presence of $\text{N}(\text{CH}_3)_4^+$ (Figure 4). Raman spectra between 980 cm^{-1} and 1140 cm^{-1} were fit to a series of Voigt peaks due the combined Gaussian and

Lorentzian contribution to the Raman signal in solution measurements [23, 24]. Peak variables of position, height, and WHH (for both Gaussian and Lorentzian components) were allowed to vary independently and residuals were used to assess the goodness of fit.

The region of the Raman spectrum containing the non-bridging phosphate oxygens symmetric stretch of DMP in the absence of added ions is well-described by three peaks centered at 1045 cm^{-1} , 1066 cm^{-1} and 1084 cm^{-1} , consistent with the positions of the overlapping $\nu_s\text{PO}_2^-$, $\nu_s\text{CO}$, and $\nu_a\text{CO}$ vibrational modes established in previous studies (Figure 4A, Table 1 Supplementary Information). The Raman spectrum for DMP in the presence $3\text{M N}(\text{CH}_3)_4^+$ can also be fit by a minimum of three peaks, but requires changes in individual peak parameters of $\nu_s\text{PO}_2^-$, $\nu_s\text{CO}$, and $\nu_a\text{CO}$ from those observed in the absence of $3\text{M N}(\text{CH}_3)_4^+$ (Figure 4B, Figure S1, Table 1, Supplementary Information). Compared to DMP in the absence of added ion, the peak for $\nu_s\text{PO}_2^-$ in $3\text{M N}(\text{CH}_3)_4^+$ is both reduced in intensity and shifted to higher wavenumbers while the adjacent peaks for $\nu_s\text{CO}$, and $\nu_a\text{CO}$ increase in intensity but remain fixed with respect to peak position. These data are consistent with the apparent change in $\nu_s\text{PO}_2^-$ position and enhancement of $\nu_s\text{CO}$, and $\nu_a\text{CO}$ signals observed in difference spectra (Figure 3). We observed, however, that when successive DMP samples were monitored within an individual Raman experiment that the variability of the $\nu_s\text{PO}_2^-$ peak position could be reduced to approximately 0.1 cm^{-1} , and thus could be used to obtain at least a qualitative understanding of the dependence of $\nu_s\text{PO}_2^-$ peak position as a function of $\text{N}(\text{CH}_3)_4^+$ concentration over the relatively small change in peak position ($\sim 2\text{ cm}^{-1}$ between 0 and $3\text{M N}(\text{CH}_3)_4^+$). A plot of the $\nu_s\text{PO}_2^-$ peak position as a function of $\text{N}(\text{CH}_3)_4^+$ concentration is not consistent with a single displacement of $\nu_s\text{PO}_2^-$ in the presence of $\text{N}(\text{CH}_3)_4^+$, but rather a progressive shift of $\nu_s\text{PO}_2^-$ to higher wavenumbers with increasing concentrations of $\text{N}(\text{CH}_3)_4^+$ (Figure 4C). This trend is observed independent of the order in which sample concentrations are measured and is consistent with the apparent change in the position of the inflection in Raman difference spectra with increasing ionic strength (compare Figures 3A and 4C).

The $\nu_s\text{PO}_2^-$ region of the Raman spectrum for DMP in the presence 3M NH_4^+ can also be fit with a minimum of three peaks, but requires changes in peak parameters for $\nu_s\text{PO}_2^-$ and $\nu_s\text{CO}$ from those observed in the absence of added ion, while peak parameters for $\nu_a\text{CO}$ remain constant. (Figure 5a, Figures S2 and S3, Supplementary Information). However, as noted above, previous studies have indicated that H-bonding to non-bridging phosphate oxygens produces a discrete change in the position of $\nu_s\text{PO}_2^-$ in the Raman spectrum for DMP and DEP [16, 18]. Fitting the raw spectral data for DMP in the presence 3M NH_4^+ to four peaks yields the putative new vibrational mode (defined here as $\nu_s\text{PO}_2\text{-H}$) 5 wavenumbers from the position of $\nu_s\text{PO}_2^-$ (Figure 5B, Table 1, Supplementary Information). This result is consistent with the displacement of $\nu_s\text{PO}_2^-$ to lower wavenumbers due to H-bonding predicted and observed in previous studies of DMP and DEP [16, 18] as well as with the apparent NH_4^+ -induced displacement of $\nu_s\text{PO}_2^-$ to lower wavenumbers observed in Raman difference spectra (Figure 3B). Thus, while three and four-peak models can both fit the observed raw spectrum equally well, the latter is more consistent with other biochemical studies.

In both the three-peak and four-peak fits of DMP in 3M NH_4^+ the combined presence of H-bonding and electrostatic interactions produce changes in the $\nu_s\text{PO}_2^-$, $\nu_s\text{CO}$ and $\nu_a\text{CO}$ vibrational modes that are distinct from that observed in the presence of electrostatic interactions alone (Figures 4 and 5). As noted above, one model to explain the observed differences is that the electrostatic interactions produce perturbations of DMP structure that are coupled to structural changes resulting from H-bonding. Alternatively, electrostatic perturbations may be sufficiently uncoupled from structural changes resulting from H-bonding to be monitored as a distinct spectroscopic signal. The first model predicts that the

contribution of electrostatic interactions to NH_4^+ -induced changes of $\nu_s\text{PO}_2^-$ cannot be predicted by changes of DMP $\nu_s\text{PO}_2^-$ in the presence of $\text{N}(\text{CH}_3)_4^+$, while the second model predicts that the electrostatic contributions from these two ions are sufficiently equivalent to allow this type of approximation.

To distinguish between these two models we examined the extent to which peak parameters observed in the presence of purely electrostatic interactions ($\text{N}(\text{CH}_3)_4^+$) could accurately predict the observed spectral data in the added presence of H-bonding (NH_4^+). Using the four peak model to analyze NH_4^+ -dependent changes in $\nu_s\text{PO}_2^-$ we observed a linear gain in the intensity (observed Raman counts in peak area) of $\nu_s\text{PO}_2^- \text{H}$ and linear loss in the intensity of $\nu_s\text{PO}_2^-$ over a range from 0.15 M to at least 3 M NH_4^+ . Loss of $\nu_s\text{PO}_2^-$ peak intensity was found to be consistently larger than that observed in the gain of $\nu_s\text{PO}_2^- \text{H}$. To test the extent to which the difference in the change in $\nu_s\text{PO}_2^-$ and $\nu_s\text{PO}_2^- \text{H}$ signals was attributable to electrostatic interactions, we measured the loss of $\nu_s\text{PO}_2^-$ intensity as a function of $\text{N}(\text{CH}_3)_4^+$ concentration (Figure 5C). The sum of the net loss of $\nu_s\text{PO}_2^-$ in the presence of $\text{N}(\text{CH}_3)_4^+$ and gain of $\nu_s\text{PO}_2^- \text{H}$ in the presence of NH_4^+ [(net $\nu_s\text{PO}_2^- \text{N}(\text{CH}_3)_4^+$ loss) + (net $\nu_s\text{PO}_2^- \text{H}^{\text{NH}_4^+}$ gain)] was found to closely approximate the total loss of $\nu_s\text{PO}_2^-$ in the presence of NH_4^+ with an average error of *ca.* 11% (Figure 5C). These data are consistent with a model in which indirect effects from different ions are small enough to allow the electrostatic contribution to be modeled independently using $\text{N}(\text{CH}_3)_4^+$, and in which the experimental signals for electrostatic ($\nu_s\text{PO}_2^-$ loss) and H-bonding ($\nu_s\text{PO}_2^- \text{H}$ gain) are sufficient to account for the total decrease in $\nu_s\text{PO}_2^-$ intensity observed in NH_4^+ . These data also suggest that H-bonding does not have a large contribution to the peak position of $\nu_s\text{PO}_2^-$ or the adjacent peaks of $\nu_s\text{CO}$ and $\nu_a\text{CO}$. Nevertheless, significant differences are observed in the apparent WHH of $\nu_s\text{PO}_2^-$, $\nu_s\text{CO}$ and $\nu_a\text{CO}$ of DMP in the presence of $\text{N}(\text{CH}_3)_4^+$ and NH_4^+ , suggesting that effects from vibrational coupling or changes in DMP geometry from structurally distinct ionic interactions do contribute to the energetic distribution of frequencies of these vibrational modes.

To test the extent to which electrostatic, H-bonding, and inner-sphere coordination could be monitored independently, we fit the raw spectrum of DMP in the presence of MgCl_2 , fixing the peak positions of $\nu_s\text{PO}_2^-$, $\nu_s\text{CO}$ and $\nu_a\text{CO}$ to those observed in $\text{N}(\text{CH}_3)_4^+$ at equal ionic strength (Figure 6, Table 1 Supplementary Information). As noted above, previous studies showed that direct coordination of phosphodiester by metal ions produces an altered vibrational mode of $\nu_s\text{PO}_2^-$ observed at higher wavenumbers[9]. The addition of a fourth peak to the fit of raw Raman spectral data for DMP in the presence 1M Mg^{2+} yields a peak that is consistent with the Mg^{2+} -dependent displacement of $\nu_s\text{PO}_2^-$ to higher wavenumbers observed in difference spectra (compare Figures 3C and 6A). The fit to four peaks, however, shows considerable error (see residuals, Figure 6A) in the region of the DMP Raman spectrum near unbound $\nu_s\text{PO}_2^-$ ($\sim 1084 \text{ cm}^{-1}$), indicating that in addition to $\nu_s\text{PO}_2^-$, $\nu_s\text{CO}$ and $\nu_a\text{CO}$, a vibrational mode associated with purely inner-sphere coordination (defined here as $\nu_s\text{PO}_2^- \text{M}$) is not sufficient to account for the observed $\nu_s\text{PO}_2^-$ region of DMP Raman spectrum in the presence of Mg^{2+} . In contrast, a fit of five peaks to the raw Raman spectral data for DMP in the presence 1M Mg^{2+} leads to a better fit to the observed Raman signal near $\nu_s\text{PO}_2^-$ throughout the 980 cm^{-1} to 1140 cm^{-1} spectral region (Figure 6B). The two peaks in addition to $\nu_s\text{PO}_2^-$, $\nu_s\text{CO}$ and $\nu_a\text{CO}$ are displaced from unbound $\nu_s\text{PO}_2^-$ to higher or lower wavenumbers consistent with that predicted for $\nu_s\text{PO}_2^- \text{M}$ and $\nu_s\text{PO}_2^- \text{H}$ in Raman difference spectra (Figures 3B, 3C), peak fits of $\nu_s\text{PO}_2^- \text{H}$ observed for NH_4^+ -induced changes of DMP $\nu_s\text{PO}_2^-$ (Figure 5B), as well as the findings of previous from experimental and theoretical studies[16, 18].

Measurement of Mg^{2+} -dependent changes in $\nu_s\text{PO}_2^-$, $\nu_s\text{PO}_2^- \text{M}$ and $\nu_s\text{PO}_2^- \text{H}$ peak intensity over a concentration range equivalent in ionic strength (0.3-3 M) to that used to monitor

changes of the Raman spectrum of DMP in the presence of $\text{N}(\text{CH}_3)_4^+$ and NH_4^+ reveals a linear concentration-dependent loss of $\nu_s\text{PO}_2^-$, and proportional gains in both $\nu_s\text{PO}_2^-M$ and $\nu_s\text{PO}_2^-H$ (Figure 6C). The observed concentration-dependent increase in $\nu_s\text{PO}_2^-M$ peak intensity is roughly twice that observed for $\nu_s\text{PO}_2^-H$ and independently measured levels for the net loss of $\nu_s\text{PO}_2^-$ in the presence of $\text{N}(\text{CH}_3)_4^+$. The sum of the Raman signals for intensities for $\nu_s\text{PO}_2^-M$ and $\nu_s\text{PO}_2^-H$ observed in Mg^{2+} and the net loss of $\nu_s\text{PO}_2^-$ in the presence of $\text{N}(\text{CH}_3)_4^+$ nevertheless closely approximates total loss of $\nu_s\text{PO}_2^-$ observed in the presence of Mg^{2+} [(net $\nu_s\text{PO}_2^-M^{\text{Mg}}$ loss) = (net $\nu_s\text{PO}_2^-N(\text{CH}_3)_4$ loss) + (net $\nu_s\text{PO}_2^-H^{\text{Mg}}$ + $\nu_s\text{PO}_2^-M^{\text{Mg}}$ gain)] with an observed experimental error of *ca.* 11%. Thus, consistent with the findings in NH_4^+ , the total Mg^{2+} -induced change in the Raman signal for $\nu_s\text{PO}_2^-$ in DMP can be accounted for by the independent and additive contributions of the spectroscopic signals for electrostatic interaction, H-bonding, and inner-sphere coordination.

3.3. Spectroscopic signals for outer-sphere and inner-sphere coordination correlate with metal ion absolute electronegativity and absolute hardness

Metal ion binding is strongly linked to the physical properties of ionization potential and electron affinity which are incorporated into the chemical properties of absolute electronegativity and absolute hardness[25]. Higher values of absolute electronegativity and absolute hardness are predicted to correlate with greater degrees of inner-sphere coordination to the phosphodiester monoanion. Thus, to examine the extent to which spectroscopic signals for inner-sphere and outer-sphere coordination in DMP reflect this chemical correlation we determined the relative levels of $\nu_s\text{PO}_2^-M$ and $\nu_s\text{PO}_2^-H$ in DMP in the presence of alkali, alkaline earth, and transition metals that represent a broad range of values for absolute electronegativity and absolute hardness (Figure 7, individual raw spectra and peak fits for all DMP metal ion pairs are provided in Figures S3 and S4). Given that the observed metal-dependent changes in DMP $\nu_s\text{PO}_2^-$ levels can be determined from the sum of spectroscopic signals for electrostatic, outer-sphere, and inner-sphere interactions, we estimated the fraction of phosphodiesters involved in inner-sphere coordination, f_{coord} , from the intensity of $\nu_s\text{PO}_2^-M$ in the presence of metal ion relative to the total DMP $\nu_s\text{PO}_2^-$ signal observed in the absence of metal ion ($f_{\text{coord}} = \nu_s\text{PO}_2^-M / \text{total } \nu_s\text{PO}_2^- \text{ no metal}$). Levels of f_{coord} are predicted to vary directly with the affinity of the metal ion. Consistent with this prediction, we find that increasing DMP f_{coord} values for metal ions compared at equal ionic strength (3M) strongly correlate with increasing values of absolute electronegativity and absolute hardness. This correlation is observed for all alkali and alkaline earth metals tested but does not hold for transition metals (Figures 7A and 7B). With the exception of Mn^{2+} and Li^+ , DMP f_{coord} values for alkali, alkaline earth, as well as transition metals, however, do correlate with measured enthalpies for metal hydration, supporting the interpretation that all measured values of f_{coord} reflect inner-sphere coordination (Figure 7C).

To examine the extent to which outer-sphere spectroscopic signals are also consistent with the chemical properties of individual metal ions we examined the fraction of inner-sphere coordination relative to the total level of observed coordination [$\nu_s\text{PO}_2^-M / (\nu_s\text{PO}_2^-H + \nu_s\text{PO}_2^-M)$] as a function of absolute electronegativity, absolute hardness, and ΔH hydration (Figure 7D-E). Higher values of absolute electronegativity, absolute hardness, and ΔH hydration are predicted to correlate with lower relative levels of outer-sphere coordination. With the exception of Ca^{2+} , this prediction appears to hold for the alkali and alkaline earth metals, while the measured signal for outer-sphere coordination in transition metals is significantly lower and shows a weaker dependence on absolute electronegativity and absolute hardness than its alkali and alkaline earth counter parts.

4. Discussion

In the current study we attempted to more clearly define the quantitative contribution of electrostatic, outer-sphere and inner-sphere interactions to the Raman signal for non-bridging phosphate oxygens ($\nu_s\text{PO}_2^-$) in the simple phosphodiester DMP. To achieve this goal we characterized changes in the Raman spectrum of DMP $\nu_s\text{PO}_2^-$ that were linked to electrostatic and outer-sphere interactions in previous quantitative studies of Ni-dependent changes of the Raman spectrum of DEP, and in computational simulations of Mg^{2+} and Ca^{2+} binding to DMP [16, 18]. Consistent with these previous studies, we observed changes in the frequency of $\nu_s\text{PO}_2^-$ to higher wavenumbers in the Raman spectrum in the presence of ions capable of only electrostatic interactions [$\text{N}(\text{CH}_3)_4^+$], and lower wavenumbers in the presence of ions also capable of outer-sphere interactions [NH_4^+] (Figures 2A, 2B, 3B, and 4B). Our findings, however, are inconsistent with the previous prediction of electrostatic interactions producing an additional $\nu_s\text{PO}_2^-$ vibrational mode approximately 10 cm^{-1} higher in the Raman spectrum [16]. Electrostatic changes to $\nu_s\text{PO}_2^-$ are consistent with a distinct physical basis for ion interaction relative to that for outer-sphere and inner-sphere coordination in which electrostatic interactions shift $\nu_s\text{PO}_2^-$ to higher wavenumbers progressively as a function ionic strength due to field effects while outer-sphere and inner-sphere coordination produces discrete changes $\nu_s\text{PO}_2^-$ frequency in a manner consistent with equilibrium binding. In addition, similar electrostatic contributions to DMP $\nu_s\text{PO}_2^-$ intensity can be observed for different ions, while the relative contribution of outer-sphere and inner-sphere coordination are strongly dependent on ion type. The magnitude of the $\nu_s\text{PO}_2^-$ frequency shift ($\sim 2\text{ cm}^{-1}$ at 3 M ionic strength, Figure 3C) is also smaller than that observed for H-bonding ($\sim 5\text{ cm}^{-1}$) and much smaller than those observed for direct coordination ($\sim 14\text{--}20\text{ cm}^{-1}$), consistent with the prediction from computational studies that changes in $\nu_s\text{PO}_2^-$ frequency should become smaller with increasing distance between the ion and DMP [18].

We find that the loss of $\nu_s\text{PO}_2^-$ signal due to electrostatic interactions combined with the increase in spectroscopic signals of $\nu_s\text{PO}_2^- \text{H}$ and $\nu_s\text{PO}_2^- \text{M}$ is sufficient to account for the total change in $\nu_s\text{PO}_2^-$ intensity from electrostatic, outer-sphere and inner-sphere interactions in the presence of Mg^{2+} and a variety of mono and divalent ions (Figure 5C). The spectroscopic signals for electrostatic, outer-sphere, and inner-sphere interactions thus appear to be sufficiently independent to be monitored individually. The above quantitative framework assumes that the Raman cross-section for the $\nu_s\text{PO}_2^-$, $\nu_s\text{PO}_2^- \text{H}$, and $\nu_s\text{PO}_2^- \text{M}$ vibrational modes are similar. While this assumption is not tested directly in the current study, the additive nature of the spectroscopic signals for electrostatic, outer-sphere, and inner-sphere interactions observed for a number of different ions suggests that this is, in fact, the case. Measured intensities of $\nu_s\text{PO}_2^-$, $\nu_s\text{PO}_2^- \text{H}$, and $\nu_s\text{PO}_2^- \text{M}$ under the conditions described above can thus be used to provide a simple quantitative framework for the three distinct forms of metal-phosphodiester interaction in DMP.

We applied this framework to quantify DMP $\nu_s\text{PO}_2^- \text{M}$ and $\nu_s\text{PO}_2^- \text{H}$ intensities induced by alkali, alkaline earth, and transition metal ions representing a broad range of values of absolute electronegativity and absolute hardness. Measured values for DMP f_{coord} are observed to correlate strongly with values of absolute electronegativity and absolute hardness for alkali and alkaline earth (but not transition) metal ions in a manner consistent with predicted relative levels of inner-sphere coordination, while the opposite correlation is observed for the fractional contribution of outer-sphere coordination. Deviations from the observed correlation between the spectroscopic signals for outer-sphere and inner-sphere coordination and values for absolute electronegativity and absolute hardness are likely to be due, in part, to differences in ion affinity for DMP and solvent water. Theoretical calculations of the free energy associated with binding of Ca^{2+} and Mg^{2+} to DMP predict

lower affinity of Ca^{2+} for water relative to Mg^{2+} , and subsequently higher levels of inner sphere-coordination of DMP than expected based on a simple correlation with absolute electronegativity or absolute hardness, which we also observe in the relative intensities of $\nu_s\text{PO}_2^- \text{M}$ and $\nu_s\text{PO}_2^- \text{H}$ (Figure 7D and 7E) [18]. In addition, the increased complexities of the bonding interactions for larger metal ions, particularly the transition metals, is likely to muddle the simple correlation between the spectroscopic signals for outer-sphere and inner-sphere coordination and chemical properties such as absolute electronegativity and absolute hardness. Greater complexity in transition metal binding may arise from the ability to interact through coordination numbers of either 4 or 6, an increased ability (relative to alkali and alkaline earth metals) to form bidentate interactions, and the added presence of *d*-orbitals which may uniquely alter the frequency, polarizability, and coupling of individual phosphodiester vibrational modes. While the region of the Raman spectrum encompassing $\nu_s\text{PO}_2^-$ in the presence of transition metals can be fit with the same peak profile ($\nu_s\text{PO}_2^- \text{M}$, $\nu_s\text{PO}_2^- \text{H}$, $\nu_s\text{PO}_2^-$, $\nu_s\text{CO}$, and $\nu_s\text{CO}$) as in alkali and alkaline earth metals, the distinct elements of the binding interactions involving transition metals may offset or alter spectroscopic sensitivity to ion effects from electrostatic, H-bonding, or inner-sphere interactions. Thus, interpretation of $\nu_s\text{PO}_2^- \text{M}$ and $\nu_s\text{PO}_2^- \text{H}$, particularly with transition metals, should be done with caution.

For the majority of ions observed under physiological conditions however, the above experimental approach provides a much-needed experimental tool for the quantification of ion interaction detected by other biophysical methods and for the experimental validation and refinement of theoretical models of ion interactions. Differences in the observed levels of coordination for different ions can also provide a basis for the potential identification of specific metal species or the distinction between different metal-phosphodiester interactions (*e.g.* Mg vs. Na) in mixed metal studies. Metal-induced changes to $\nu_s\text{PO}_2^-$ in DMP have been shown to be highly similar to that observed in nucleic acids and other phosphodiester model systems and thus comparative analysis of outer-sphere and inner-sphere coordination from $\nu_s\text{PO}_2^- \text{M}$, $\nu_s\text{PO}_2^- \text{H}$, and $\nu_s\text{PO}_2^-$ should also hold for more complex phosphodiesters[9]. Measurement of $\nu_s\text{PO}_2^- \text{M}$ and $\nu_s\text{PO}_2^- \text{H}$ by peak fitting of the observed Raman spectrum, however, is difficult under conditions where the fraction of coordinated phosphodiester (f_{coord}) is small ($< 1\text{-}2\%$, Figure 6). Levels of metal coordination, however, can be higher at specific phosphodiesters within a larger structure and can be isolated by site-specific atomic or isotopic substitution[26, 27]. Alternatively, information about the effects of electrostatic or coordination interactions may be obtained from the quantitative analysis of the attenuation of the large $\nu_s\text{PO}_2^-$ signal itself. Ion-dependent attenuation of $\nu_s\text{PO}_2^-$ is readily apparent in the Raman spectra nucleic acids [9, 10, 13, 14, 16, 28] and can be combined with the analysis of Raman difference spectra under conditions where peak fitting is difficult.

Supplementary Material

Refer to Web version on PubMed Central for supplementary material.

Acknowledgments

We thank Paul Carey, David Draper, Victoria DeRose, Janet Morrow, and George Thomas Jr., for insightful comment and helpful discussion. This work was supported by NIH GM56740 to MEH.

References

1. Misra VK, Draper DE. Biopolymers. 1998; 48:113–135. [PubMed: 10333741]
2. Sigel RK, Pyle AM. Chem Rev. 2007; 107:97–113. [PubMed: 17212472]

3. Feig, AL.; Uhlenbeck, OC. *The RNA World*. Cech, T.; Gesteland, R.; Atkins, J., editors. Vol. 2. Cold Spring Harbor Laboratory Press; Cold Spring Harbor, NY: 1999. p. 287-320.
4. Lilley DM. *Curr Opin Struct Biol*. 2005; 15:313–323. [PubMed: 15919196]
5. Draper DE. *Biophys J*. 2008; 95:5489–5495. [PubMed: 18835912]
6. Bai Y, Greenfeld M, Travers KJ, Chu VB, Lipfert J, Doniach S, Herschlag D. *J Am Chem Soc*. 2007; 129:14981–14988. [PubMed: 17990882]
7. Draper DE, Grilley D, Soto AM. *Annu Rev Biophys Biomol Struct*. 2005; 34:221–243. [PubMed: 15869389]
8. Misra VK, Draper DE. *J Mol Biol*. 2002; 317:507–521. [PubMed: 11955006]
9. Christian EL, Anderson VE, Carey PR, Harris ME. *Biochemistry*. 2010; 49:2869–2879. [PubMed: 20180599]
10. Gong B, Chen Y, Christian EL, Chen JH, Chase E, Chadalavada DM, Yajima R, Golden BL, Bevilacqua PC, Carey PR. *J Am Chem Soc*. 2008; 130:9670–9672. [PubMed: 18593125]
11. Carey, PR. *Biochemical Applications of Raman and resonance Raman Spectroscopies*. Academic Press Inc.; New York, NY: 1982.
12. Spiro, TG. *Biological Applications of Raman Spectroscopy*. John Wiley & Sons Ins.; New York, NY: 1987.
13. Duguid J, Bloomfield VA, Benevides J, Thomas GJ Jr. *Biophys J*. 1993; 65:1916–1928. [PubMed: 8298021]
14. Langlais M, Tajmir-Riahi HA, Savoie R. *Biopolymers*. 1990; 30:743–752. [PubMed: 2275976]
15. Lanir A, Yu NT. *J Biol Chem*. 1979; 254:5882–5887. [PubMed: 447685]
16. Stangret J, Savoie R. *Can. J. Chem*. 1992; 70:2875–2883.
17. Takeuchi H, Murata H, Harada I. *J. Am. Chem. Soc*. 1988; 110:392–397.
18. Petrov AS, Funseth-Smotzer J, Pack GR. *Int. J. of Quant. Chem*. 2007; 1-2:645–655.
19. Guan Y, Wurrey CJ, Thomas GJ Jr. *Biophys J*. 1994; 66:225–235. [PubMed: 8130340]
20. Guan Y, Choy GS-C, Rainer Glaser R, Thomas GJ Jr. *J. Phys. Chem*. 1995; 99:12054–12062.
21. Guan Y, Thomas GJ Jr. *Biopolymers*. 1996; 39:813–835. [PubMed: 8946802]
22. Guan Y, Thomas GJ Jr. *J. Mol. Struct*. 1996; 379:31–41.
23. Rothschild, WG. *Dynamics of Molecular Liquids*. John Wiley and Sons; New York: 1984.
24. Pelikán, P.; Ceppan, M.; Liska, M. *Applications of Numerical Methods in Molecular Spectroscopy*. CRC Press; Boca Raton: 1993.
25. Pearson RG. *Inorg. Chem*. 1988; 27:734–740.
26. Chen JH, Gong B, Bevilacqua PC, Carey PR, Golden BL. *Biochemistry*. 2009; 48:1498–1507. [PubMed: 19178151]
27. Chen Y, Eldho NV, Dayie TK, Carey PR. *Biochemistry*. 2010; 49:3427–3435. [PubMed: 20225830]
28. Gong B, Chen JH, Bevilacqua PC, Golden BL, Carey PR. *Biochemistry*. 2009; 48:11961–11970. [PubMed: 19888753]
29. Richens, DT. *The Chemistry of Aqua Ions*. John Wiley & Sons Ins.; New York, NY: 1997.

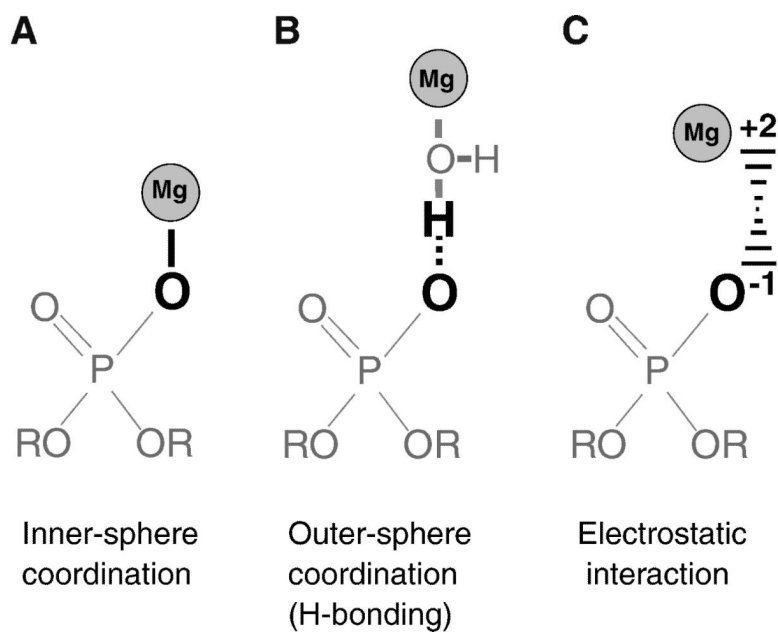


Figure 1. Modes of metal-phosphodiester interaction

Schematic of inner-sphere, outer-sphere, and electrostatic metal ion (shown as Mg^{2+}) interactions with the non-bridging phosphate oxygens of a phosphodiester. The partial charges are indicated, however, the distribution of charge is not meant to reflect experimentally determined values.

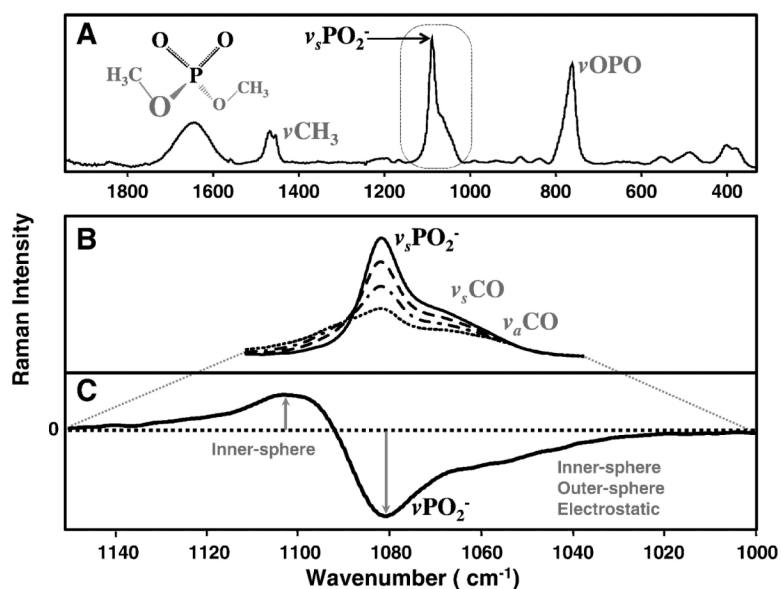


Figure 2. Metal-dependent changes in Raman spectra of non-bridging phosphate oxygens ($\nu_s\text{PO}_2^-$) of DMP

(A) Raman spectrum (observed photon counts from 300 cm^{-1} to 1900 cm^{-1}) for 0.2 M DMP highlighting the major peaks of the methyl group (νCH_3), and the symmetric non-bridging ($\nu_s\text{PO}_2^-$) and bridging ($\nu_s\text{OPO}$) phosphate oxygen vibrational modes. A dotted square oval marks region of Raman spectrum (1000 cm^{-1} to 1150 cm^{-1}) shown in panels B and C. Inset shows molecular schematic of DMP with atoms involved in the $\nu_s\text{PO}_2^-$ vibrational mode shown in black. (B) Isolated $\nu_s\text{PO}_2^-$ and adjacent symmetric ($\nu_s\text{CO}$) and asymmetric ($\nu_a\text{CO}$) C-O bond stretches of 0.2 M DMP in the absence (solid line) and presence of 1 M (dashed line), 2 M (dot + dashed line), or 3 M (dotted line), MgCl_2 . (C) Example of Raman difference spectrum, subtracting the Raman signal of DMP in the absence of metal ion from that in the presence of 1 M MgCl_2 . The dotted line indicates Raman intensity of 0. Arrows indicate loss of $\nu_s\text{PO}_2^-$ or gain of Raman signal at higher wavenumbers in the presence of metal ion. Metal-dependent loss of $\nu_s\text{PO}_2^-$ signal in Raman difference spectra was previously shown to be linked to electrostatic, outer-sphere, and inner-sphere interactions, while gain of Raman signal at higher wavenumbers is due to purely inner-sphere interactions.

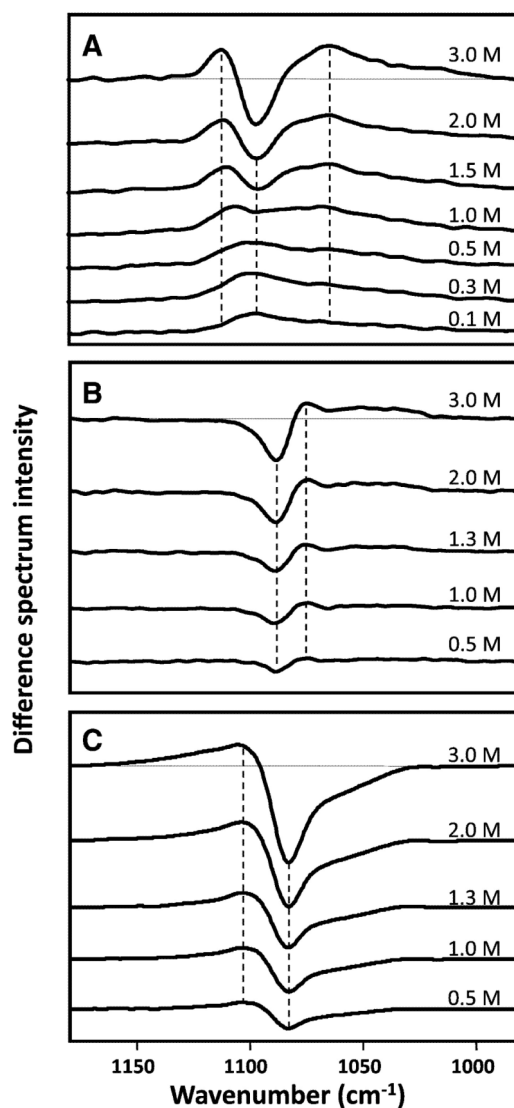


Figure 3. Dependence of Raman difference spectra of $\nu_s\text{PO}_2^-$ on ion type and concentration
 Raman difference spectra of 0.2 M DMP (980 cm^{-1} to 1180 cm^{-1}) in the presence of $\text{N}(\text{CH}_3)_4\text{Cl}$ (A), NH_4Cl (B), and MgCl_2 (C). Vertical dotted lines are drawn to facilitate comparison of the relative positions of inflection points in the difference spectra as a function of concentration. Ion concentration is expressed in molar ionic strength (M) at right and just above individual spectra. Horizontal dotted line through difference spectra at 3 M ionic strength indicates Raman difference value of zero. The Y axis (photon counts) for (A), (B), and (C) is identical in scale to facilitate comparison.

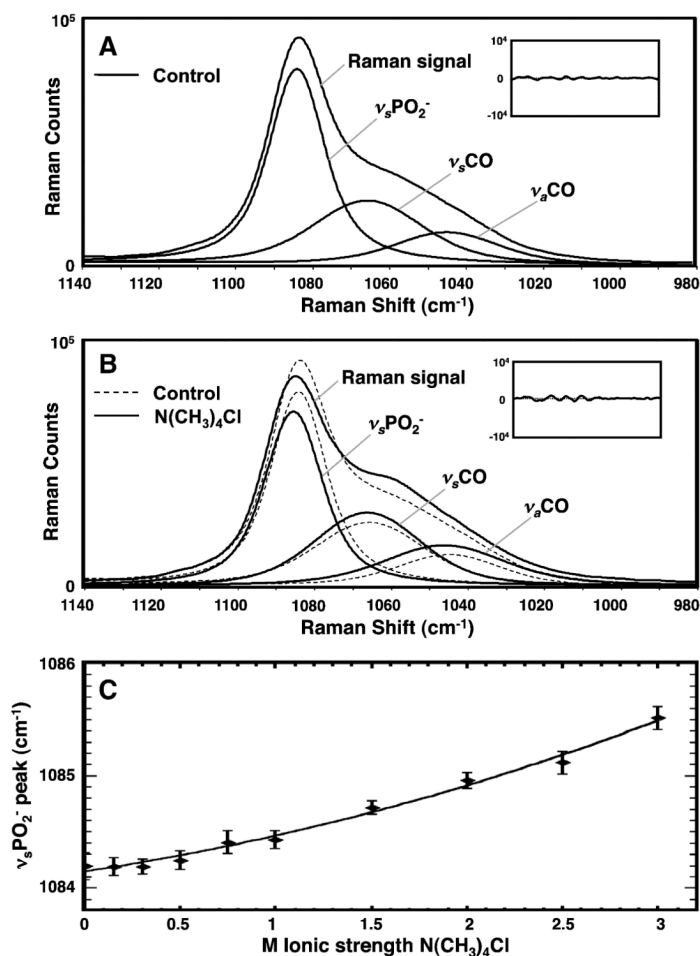


Figure 4. Effect of electrostatic interactions on $\nu_s\text{PO}_2^-$

(A) Raman spectrum (photon counts from 980 to 1140 cm^{-1}) of 0.2 M DMP fitted to Voigt peaks corresponding to $\nu_s\text{PO}_2^-$ and adjacent $\nu_s\text{CO}$ and $\nu_a\text{CO}$ vibrational modes in 0.2 M formate buffer pH 6.0. Inset reflects residuals from the subtraction of the calculated peaks from the observed Raman spectrum. Residuals are shown at a scale five times larger than the observed DMP spectral data. (B) Raman spectrum of 0.2 M DMP in the added presence of 3 M $\text{N}(\text{CH}_3)_4\text{Cl}$ fitted to Voigt peaks corresponding to $\nu_s\text{PO}_2^-$, $\nu_s\text{CO}$, and $\nu_a\text{CO}$ (solid lines) with residuals as described in (A). Dashed lines represent data shown in (A) to reveal changes in the DMP Raman spectrum induced by $\text{N}(\text{CH}_3)_4\text{Cl}$. (C) Dependence of $\nu_s\text{PO}_2^-$ peak position (diamonds) as a function of molar ionic strength (M) $\text{N}(\text{CH}_3)_4\text{Cl}$. Line represents least squares polynomial fit to highlight the concentration dependent change in $\nu_s\text{PO}_2^-$ peak position.

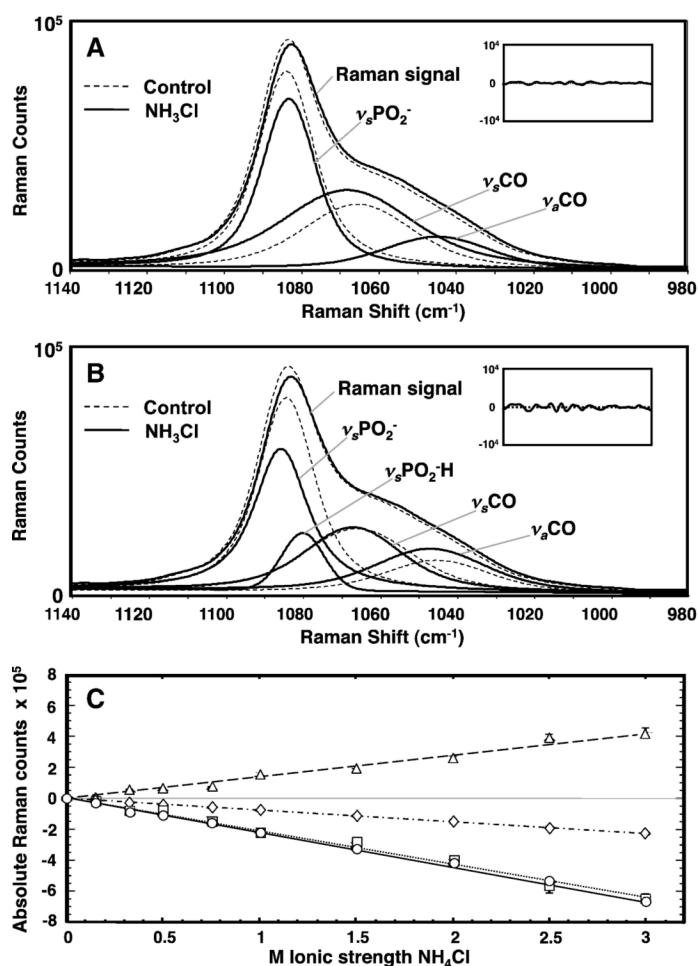


Figure 5. Effect of electrostatic and H-bonding interactions on $\nu_s\text{PO}_2^-$
 (A) Raman spectrum (photon counts from 980 to 1140 cm^{-1}) of 0.2 M DMP in 3 M NH_4Cl , 0.2 M formate buffer pH 6.0 fitted to Voigt peaks (solid lines) corresponding to the vibrational modes of $\nu_s\text{PO}_2^-$, $\nu_s\text{CO}$, and $\nu_a\text{CO}$. Dashed lines represent data shown in Figure 3A to reveal changes in the DMP Raman spectrum induced by NH_4Cl . Inset reflects residuals as described in Figure 3. (B) Raman spectrum in (A) fit with Voigt peaks corresponding to $\nu_s\text{PO}_2^-$, $\nu_s\text{CO}$, $\nu_a\text{CO}$ and an additional Voigt peak corresponding to outer-sphere coordination, $\nu_s\text{PO}_2\text{H}$. Dashed lines represent DMP Raman spectrum in the absence of NH_4Cl as described in (A). (C) Additive effects of electrostatic interactions and H-bonding. $\text{N}(\text{CH}_3)_4\text{Cl}$ - or NH_4Cl -dependent loss of $\nu_s\text{PO}_2^-$ peak intensity (diamonds or circles, respectively) is plotted as a function of molar ionic strength. Triangles reflect NH_4Cl -dependent gain of $\nu_s\text{PO}_2\text{H}$ peak intensity. The sum of independently measured values for $\nu_s\text{PO}_2^-$ loss in the presence of $\text{N}(\text{CH}_3)_4\text{Cl}$ (electrostatic interactions, diamonds) and $\nu_s\text{PO}_2\text{H}$ gain in the presence of NH_4Cl (H-bonding, triangles) at the same ionic strength is marked as square and is expressed as a loss (negative sum, squares) to facilitate quantitative comparison to the observed loss of $\nu_s\text{PO}_2^-$ in the presence of NH_4Cl (circles). Lines represent linear least squares fits to peak intensity values.

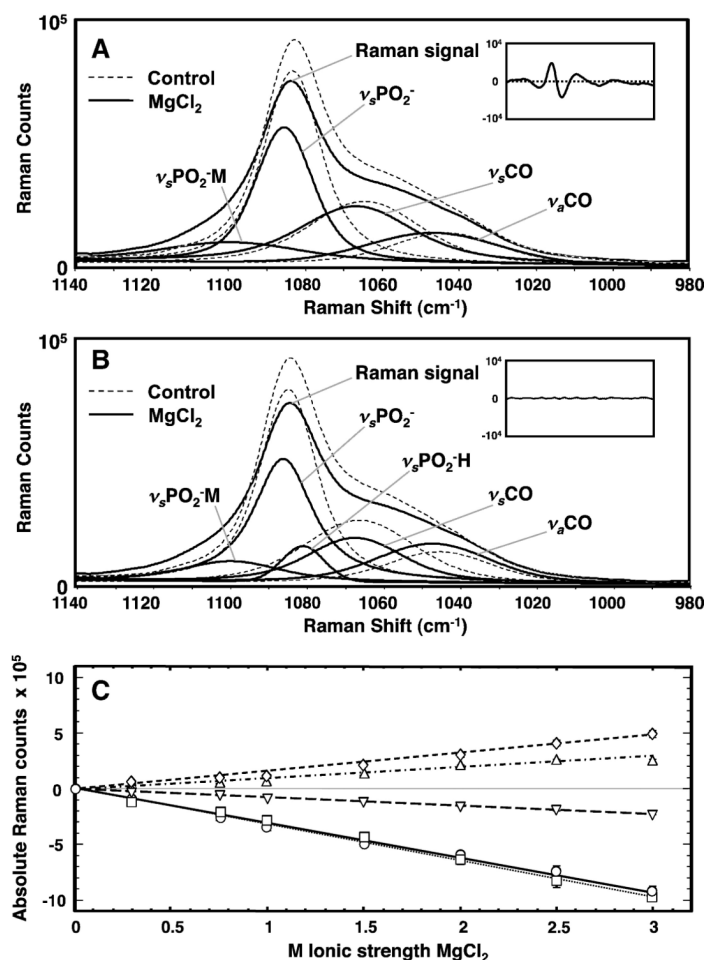


Figure 6. Effect of electrostatic, H-bonding, and inner-sphere interactions on $\nu_s\text{PO}_2^-$
 (A) Raman spectrum (photon counts from 980 to 1140 cm⁻¹) of 0.2M DMP in 1 M MgCl₂, 0.2 M formate buffer pH 6.0 fitted to Voigt peaks (solid lines) corresponding to the vibrational modes of $\nu_s\text{PO}_2^-$, $\nu_s\text{CO}$, $\nu_a\text{CO}$, and $\nu_s\text{PO}_2\text{-M}$. Inset describes Voigt fit residuals as described in Figures 3 and 4. Dotted lines represent data shown in Figure 3A to reveal changes in the DMP Raman spectrum induced by MgCl₂. (B) Raman spectrum in (A) fit with Voigt peaks corresponding to $\nu_s\text{PO}_2^-$, $\nu_s\text{CO}$, $\nu_a\text{CO}$, $\nu_s\text{PO}_2\text{-M}$, and $\nu_s\text{PO}_2\text{-H}$. Inset and dotted black lines are as described in (A). (C) Additive effects of electrostatic, H-bonding, and inner-sphere interactions. N(CH₃)₄Cl or MgCl₂-dependent loss of $\nu_s\text{PO}_2^-$ peak intensity (inverted triangles or circles, respectively) is plotted as a function of molar ionic strength. MgCl₂-dependent gain of $\nu_s\text{PO}_2\text{-H}$ and $\nu_s\text{PO}_2\text{-M}$ are expressed as triangles and diamonds respectively. The sum of independently measured values for loss of $\nu_s\text{PO}_2^-$ in the presence of N(CH₃)₄Cl (electrostatic interactions, inverted triangles), and gain in $\nu_s\text{PO}_2\text{-H}$ (H-bonding, triangles) and $\nu_s\text{PO}_2\text{-M}$ (inner-sphere coordination, diamonds) in the presence of MgCl₂ at the same ionic strength is marked as a square and is expressed as a loss (negative sum, squares) to facilitate quantitative comparison to the observed loss of $\nu_s\text{PO}_2^-$ in the presence of MgCl₂ (circles). Lines represent least-of-squares linear fits to peak intensity values.

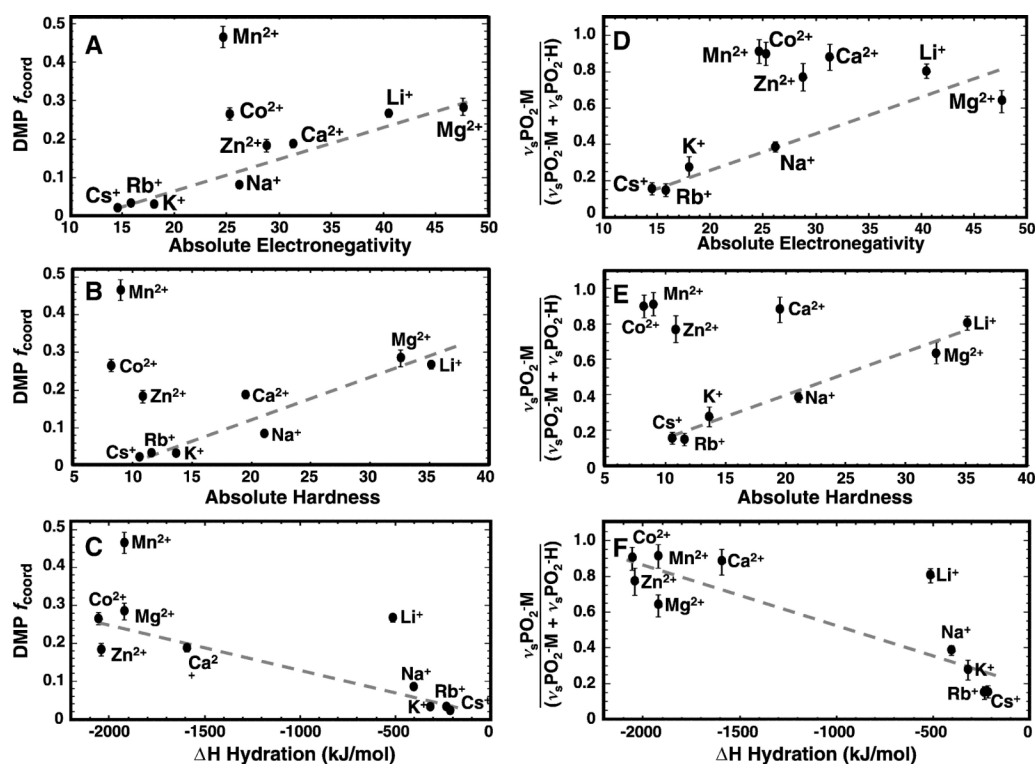


Figure 7. Dependence of inner- and outer-sphere coordination on electronegativity, hardness, and ΔH hydration

(A) Dependence of the fraction of total DMP $\nu_3\text{PO}_2^-$ signal involved in direct coordination, $\text{DMP } f_{\text{coord}}$, on absolute electronegativity. $\text{DMP } f_{\text{coord}}$ is equal to the observed signal (photon counts) for inner-sphere coordination in the presence of metal ion, $\nu_3\text{PO}_2^-M$, divided by the total $\nu_3\text{PO}_2^-$ signal in the absence of added metal ion. Values were derived from Raman spectral analysis of 0.2 M DMP in the presence of alkali, alkaline earth, and transition metals at 3 M ionic strength plotted as a function of metal ion absolute electronegativity as defined by Pearson[25]. (B) Dependence of $\text{DMP } f_{\text{coord}}$ on absolute hardness as defined by Pearson[25]. (C) Dependence of $\text{DMP } f_{\text{coord}}$ on metal ion hydration enthalpies as defined by Richens[29]. Error bars reflect standard error from at least three experiments. (D) Dependence of the fraction of total coordination attributed to inner-sphere interactions on absolute electronegativity. Total coordination attributed to inner-sphere interactions is calculated from the observed signal (photon counts) for the spectroscopic signal for inner-sphere coordination divided by the total signal for inner-sphere and outer-sphere coordination [$\nu_3\text{PO}_2^-M / (\nu_3\text{PO}_2^-M + \nu_3\text{PO}_2^-H)$]. Values were derived from Raman spectral analysis of 0.2 M DMP in the presence of alkali, alkaline earth, and transition metals at 3 M ionic strength plotted as a function of metal ion absolute electronegativity as described in Figure 6. (E) Dependence [$\nu_3\text{PO}_2^-M / (\nu_3\text{PO}_2^-M + \nu_3\text{PO}_2^-H)$] on absolute hardness as defined by Pearson[25]. (F) Dependence of [$\nu_3\text{PO}_2^-M / (\nu_3\text{PO}_2^-M + \nu_3\text{PO}_2^-H)$] on metal ion hydration enthalpies as defined by Richens[29]. Error bars reflect standard error from at least three experiments.